

NaviHydra: Controllable Navigation-guided End-to-end Autonomous Driving with Hydra-distillation

1st Hanfeng Wu
Karlsruhe Institute of Technology
BMW Group
Munich, Germany
hanfeng.wu@bmw.de

2nd Marlon Steiner
Karlsruhe Institute of Technology
Karlsruhe, Germany
marlon.steiner@kit.edu

3th Michael Schmidt
BMW Group
Munich, Germany
michael.se.schmidt@bmw.de

4rd Alvaro Marcos-Ramiro¹
BMW Group
Munich, Germany
alvaro.marcos-ramiro@bmw.de

5th Christoph Stiller
Karlsruhe Institute of Technology
Karlsruhe, Germany
stiller@kit.edu

Abstract—The complexity of autonomous driving scenarios requires robust models that can interpret high-level navigation commands and generate safe trajectories. While traditional rule-based systems can react to these commands, they often struggle in dynamic environments, and end-to-end methods face challenges in complying with explicit navigation commands. To address this, we present NaviHydra, a controllable navigation-guided end-to-end model distilled from an existing rule-based simulator. Our framework accepts high-level navigation commands as control signals, generating trajectories that align with specified intentions. We utilize a Bird’s Eye View (BEV) based trajectory gathering method to enhance the trajectory feature extraction. Additionally, we introduce a novel navigation compliance metric to evaluate adherence to intended route, improving controllability and navigation safety. To comprehensively assess our model’s controllability, we design a test that evaluates its response to various navigation commands. Our method significantly outperforms baseline models, achieving state-of-the-art results in the NAVSIM benchmark, demonstrating its effectiveness in advancing autonomous driving.

Index Terms—End-to-end autonomous driving

I. INTRODUCTION

The rapid advancement of autonomous driving (AD) technology has underscored the need for robust trajectory planning systems capable of navigating complex environments. Accurate trajectory planning is crucial for ensuring the safety and efficiency of autonomous vehicles, particularly in scenarios where multiple navigation directions are permissible. In this context, we present a novel end-to-end (E2E) autonomous driving framework that takes sensor data and a navigation command as input, generating a trajectory output that ensures safety, efficiency and compliance with given navigation command.

The essence of end-to-end planning is to learn a holistic driving policy that can generalize across various situations

without the need for explicit intermediate steps. However, achieving controllability, where the vehicle’s actions align closely with high-level navigation commands, remains a significant challenge for these systems. This difficulty arises from the inherent complexity of training a single model to respond appropriately to explicit navigation commands while maintaining implicit learnable embeddings. While rule-based systems can effectively handle specific scenarios by leveraging explicit navigation inputs, they often struggle to adapt to the dynamic and complex nature of real-world environments. Traditional E2E planners [3], [6] often employ imitation learning from expert driving demonstrations, which implicitly encourages the model to learn the planning direction in conjunction with the input navigation commands. However, this training paradigm can lead to unsafe interpolation problems, resulting in unsafe behaviors during end-to-end learning [5]. To address these issues, trajectory proposal-based methods [1], [5], [12], [40] have emerged, which are distilled from an offline simulator using a fixed set of trajectory proposals. Although this approach mitigates the interpolation problem associated with imitation learning, it falls short of accurately following navigation directions, as the trajectories that do not follow input navigation command are not penalized properly. As a result, the model may struggle to maintain alignment with high-level navigation commands, limiting its effectiveness in real-world scenarios.

In this paper, we address these critical challenges by proposing a novel framework that enhances the navigation safety and controllability of end-to-end autonomous driving systems. Our method encodes the surrounding environment into BEV feature, providing a rich representation of the scene. A trajectory gathering method then aggregates the relevant grid from the BEV feature using trajectory proposals, effectively forming a trajectory query. This trajectory gathering

¹denotes corresponding author

method offers context-position-aware information, leading to significant improvements in model performance. Moreover, we introduce navigation compliance metric (NAVI), which leverages route information alongside the integration of navigation commands. With this metric in the loss function, it allows the model to respond more effectively to various navigation commands, thereby improving its controllability. Inspired by Hydra-MDP [1], the output of the trajectory decoder is subsequently processed by a hydra scorer, aligning the predicted scores for each trajectory with the sub-scores evaluated from offline simulations. To evaluate the effectiveness of our method, we introduce a novel controllability measure (CM) that assesses the model’s ability to react to different navigation commands. Extensive experiments conducted on the NAVSIM dataset demonstrate that our approach achieves state-of-the-art performance, excelling in both safety and controllability. In conclusion, the main contributions of this paper can be structured as follows:

- We introduce a novel **trajectory gathering** method in Sec. III-B that provides context-position-aware information compared with simple token-based method, improving the planning quality.
- We design a **navigation compliance metric** (NAVI) in Sec. III-C, which leverages the route information to improve the alignment between the trajectory prediction and input navigation command.
- We introduce a novel **controllability measure** (CM) in Sec. IV-B, evaluating the reactivity of model being imposed different navigation commands.
- Extensive experiments are conducted in Sec. IV to showcase our model excelling in both **navtest** and controllability evaluation in NAVSIM benchmark.

II. RELATED WORK

A. BEV representation learning

BEV representation transforms the raw sensor data from cameras and LiDAR into a top-down view, allowing for effective integration of spatial information and facilitating the understanding of complex driving scenarios. Early approaches [19], [20] leverage CNN and Inverse-Perspective-Mapping (IPM) to transform image features into the BEV. These methods typically assume a ground plane and implicitly learn the depth distribution of frustums. More recent works [16], [21]–[24], [35], [36] represented by BEVFormer [16] use transformer to aggregate image features to BEV features achieving huge success and has been the foundation of future BEV related work. For multi-modalities, multiple methods [14], [38], [39] leverage additional LiDAR information to enhance the performance of perception tasks in AD contexts.

In addition, BEV representation has been instrumental in addressing the challenges associated with world models in autonomous driving domain [26]–[28]. By representing the environment in a grid format, these models can effectively encode spatial information, allowing for a more structured and coherent representation of the scene.

B. End-to-end autonomous driving

End-to-end autonomous driving has attracted significant attention following the success of various approaches [3], [4], [6]. Methods based on BEV representations [14], [16], [25], [37] have achieved remarkable results in perception tasks within the autonomous driving domain, establishing BEV as a crucial intermediate representation in end-to-end autonomous driving (E2EAD) methods [6], [13], [17], [18], [32], [33]. Concurrently, sparse representation-based methods [1], [5], [12], [30], [31], [34] have gained popularity due to their computational efficiency and comparable performance.

In addition to advancements in representation learning, significant research has been conducted in the planning domain. Early E2EAD methods [3], [4], [6] trained planners by minimizing the distance between predicted trajectories and expert trajectories. However, as highlighted by VADv2 [5], relying on imitation learning can lead to undesirable interpolation, resulting in potentially dangerous scenarios. To address this issue, VADv2 proposed learning from the distribution of trajectory proposals rather than directly from the L2 loss associated with expert trajectories. Hydra-MDP [1], [34] builds on the concept of trajectory proposals, utilizing offline simulations to distill the model from simulated results. This approach shifts the focus from training a trajectory planner to training a trajectory scorer, effectively learning from closed-loop metrics loss instead of the conventional L2 loss.

C. Navigation-guided autonomous driving

Navigation commands serve as critical input signals for autonomous driving functions. Methods with privileged perception inputs, such as IDM [29] and PDM-closed [7] leverage the route information directly to navigate the ego vehicle. Previous work [1], [3], [10] primarily encoded navigation commands as embeddings, supplementing other ego status features. However, this simplistic integration lacks the controllability necessary for responding to different navigation commands. SSR [18] successfully incorporates navigation commands into the BEV embedding using a Squeeze-and-Excitation (SE) Layer [15] and supervises the planner through imitation learning. While this approach effectively visualizes attention variations in response to different navigation commands, it falls short of demonstrating the model’s navigation controllability due to its reliance on a straightforward imitation learning strategy.

III. METHODS

As depicted in Fig. 1, the proposed NaviHydra framework consists of three primary components: a scene feature extractor (Sec. III-A), a trajectory decoder (Sec. III-B), and a hydra distillation (Sec. III-C). We address each of them accordingly. In addition, the inference protocol is introduced in Sec. III-D.

A. Scene feature extractor

The scene feature extractor is responsible for encoding the surrounding images and LiDAR data into the BEV space, obtaining BEV features \mathbf{B}^{origin} to represent the scene context.

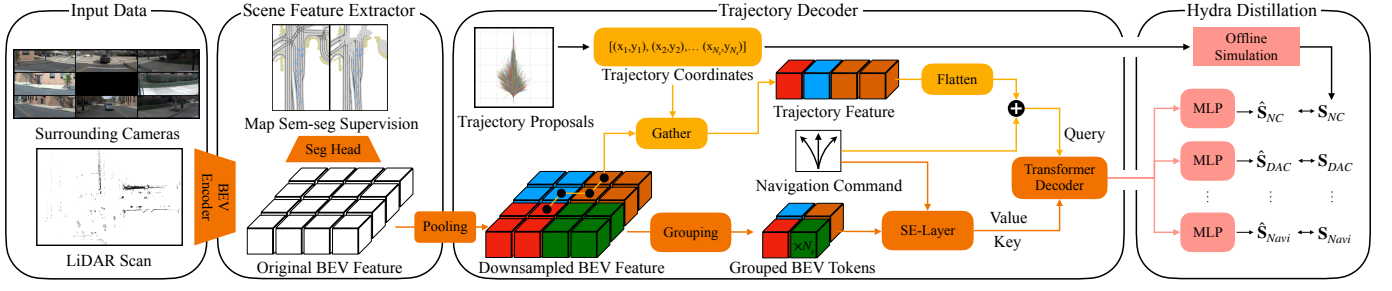


Fig. 1. Overview of our method. We encode the surrounding camera images and LiDAR point clouds into a BEV feature. The BEV encoder is pretrained using a semantic segmentation task. For the trajectory decoder, we gather the corresponding grid from the BEV feature using the trajectory proposal to construct the trajectory query. The navigation command is integrated into the BEV feature to create the key and value inputs. The output of the trajectory decoder is then fed into a hydra scorer to align with each sub-score from the offline simulation.

We utilize a semantic segmentation task based on a straightforward convolutional head to pretrain the scene feature extractor. The design of the perception network aims to effectively extract single-frame semantic information from available ground-truth labels.

B. Trajectory decoder

We utilize BEV features to construct the query, key, and value inputs for the transformer decoder, which subsequently outputs the final trajectory features for use in the next stage. This section details how the model: 1) tokenizes BEV features into sparse tokens that serve as keys and values for the transformer decoder, 2) generates the trajectory query for the transformer decoder, 3) incorporates navigation commands into the input of the transformer decoder, and 4) decodes the final trajectory feature.

a) BEV features tokenizer.: It is designed to tokenize the original BEV feature \mathbf{B}^{origin} to obtain position- and context-sensitive tokens that function as keys and values for the transformer decoder. The original BEV feature has a dense shape of $240 \times 160 \times 512$ (H \times W \times C) which is computationally inefficient to be used directly as input to the transformer decoder. To effectively aggregate the information while preserving the positional relationships among the grids, we first apply max pooling to the original BEV feature to create a downsampled BEV feature \mathbf{B}^{down} . Subsequently, we group every N_s neighboring BEV grids into BEV tokens $\mathbf{B}^{grouped}$, where N_s is selected as the number of waypoints to align the feature dimensions with the trajectory features.

b) Trajectory gathering.: It is employed to acquire the trajectory features that will serve as query inputs for the transformer decoder. We follow Hydra-MDP [1] to collect all ego-centric trajectory data points from the entire dataset and cluster them into N_t trajectory proposals $\{\mathbf{T}_i\}_{i=1}^{N_t}$. For each trajectory proposal $\mathbf{T}_i \in \{\mathbf{T}_i\}_{i=1}^{N_t}$, where $\mathbf{T}_i = \{(x_i^s, y_i^s, \theta_i^s)\}_{s=1}^{N_s}$ with N_s representing the number of trajectory waypoints, we gather the trajectory feature \mathbf{F}_i from the corresponding grid of the downsampled BEV feature \mathbf{B}^{down} based on the waypoint coordinates of the trajectory:

$$\mathbf{F}_i = \text{flatten}(\{\mathbf{B}^{down}(x_i^s, y_i^s)\}_{s=1}^{N_s}). \quad (1)$$

Each BEV grid from downsampled BEV feature \mathbf{B}^{down} has a larger receptive field compared to the BEV grid from the original BEV feature \mathbf{B}^{origin} , so that the gathered trajectory feature can efficiently preserve more spatial context information of the surrounding environment.

c) Integrating navigation commands.: To enhance the controllability of the model, it is essential to integrate navigation command information into the model and establish a loss function to supervise the end-to-end training of navigation compliance. Provided by the NAVSIM dataset, navigation commands $C = \{\text{Turn Left}, \text{Go Straight}, \text{Turn Right}\}$ are represented using three learnable embeddings. An SE layer [15] is employed to fuse these navigation command embeddings with the grouped BEV feature $\mathbf{B}^{grouped}$, resulting in a navigation-aware BEV feature, which has the same dimension as $\mathbf{B}^{grouped}$, defined as $\mathbf{B}^{navi} = \text{SE}(\mathbf{B}^{grouped}, c)$, where $c \in C$. Additionally, the navigation command embedding is added to the trajectory feature \mathbf{F}_i . This integration of navigation command information not only enhances the model's ability to respond to high-level navigation inputs, but also improves overall planning performance, thereby facilitating safer and more effective autonomous driving.

d) Transformer decoder.: The trajectory feature \mathbf{F}_i , captures the positional and kinetic characteristics with limited surrounding information of the proposed trajectory. In order to enhance it with more contextual information, we utilize a transformer decoder block that integrates richer environmental information. We flatten the navigation-aware BEV feature \mathbf{B}^{navi} to construct the environmental feature \mathbf{F}_{env} . This environmental feature \mathbf{F}_{env} serves as the key and value inputs within the transformer decoder block, while the pre-calculated trajectory feature \mathbf{F}_i is employed as the query. As a result, we generate the final trajectory feature \mathbf{F}_i^{final} for each trajectory proposal $\mathbf{T}_i \in \{\mathbf{T}_i\}_{i=1}^{N_t}$ as follows.

$$\mathbf{F}_i^{final} = \text{Transformer}^1(Q = \mathbf{F}_i, K, V = \mathbf{F}_{env}) \quad (2)$$

The final trajectory features $\{\mathbf{F}_i^{final}\}_{i=1}^{N_t}$ are served as input for the hydra distillation process.

¹Represents a 3 layer decoder-only transformer architecture.

C. Hydra distillation

The hydra distillation process, inheriting from Hydra-MDP [1], takes trajectory features from the trajectory decoder as input and learns a scoring function from an existing off-line simulator for multiple closed-loop metrics. In this section, we 1) introduce the newly proposed navigation compliance metric, 2) discuss the hydra scoring process and off-line simulations using trajectory proposals, 3) explain the loss terms for distilling knowledge from simulation scores.

a) *Navigation compliance.*: To ensure navigation compliance, we utilize the route information provided in the nuPlan dataset [8]. The route of the ego vehicle in nuPlan encompasses the possible lanes leading to a predefined goal point. This includes not only the lanes traversed by the ego vehicle to reach its future destination but also parallel lanes that the vehicle may potentially use to achieve the same goal. The original NAVSIM benchmark does not penalize trajectories that result in off-route situations. For instance, in an intersection scenario, the expert trajectory turns left, while appropriate trajectories going straight or turning right can also yield successful simulation results. To align the simulation outcomes with the input navigation commands, we introduce a navigation compliance metric (NAVI), as illustrated in Fig. 2. We identify the lane IDs that are on-route and verify whether the last waypoint of the evaluated trajectory \mathbf{T}_i is located on any of those lanes. The navigation compliance metric can be formulated as follows

$$NAVI(\mathbf{T}_i = \{(x_i^s, y_i^s, \theta_i^s)\}_{s=1}^{N_s}) = \mathbf{1}_{\mathbf{L}_{route}}((x_i^{N_s}, y_i^{N_s})), \quad (3)$$

where $\mathbf{1}$ is the indicator function, \mathbf{L}_{route} is the points set representing the lanes on route. In intersection scenarios, the NAVI metric strictly aligns with the provided navigation command. However, the NAVI metric can exhibit ambiguity in lane-changing scenarios wrt. the input command. When multiple parallel lanes are on route, the NAVI metric will always be 1, regardless of which lane the ego vehicle is changing to. The design choice behind this approach is intentional: we do not want the vehicle to strictly follow the navigation command under all circumstances. Instead, the goal is for the vehicle to understand the driving intention and act reasonably in response to the navigation command to follow the route.

b) *Hydra scorer.*: The hydra scorer is a learnable feed-forward network designed to score the closed-loop performance of trajectory proposals. To train it, we employ a multi-head distillation technique [1] to establish alignment between its output and the offline simulator. The offline simulator assesses all N_t trajectory proposals within the training dataset and collects the corresponding simulation scores $\{\mathbf{S}_i^m\}_{i=1}^{N_t}$, where $M = \{NC, DAC, TTC, EP, C, NAVI\}$ denotes the set of simulation metrics, which represent Non-Collision (NC), Drivable Area Compliance (DAC), Time-to-Collision (TTC), Ego Progress (EP), Comfort (C), and Navigation Compliance (NAVI), and \mathbf{S}_i^m represents the ground truth simulation score for the i -th trajectory proposal corresponding to metric m . The final trajectory features $\{\mathbf{F}_i^{final}\}_{i=1}^{N_t}$ are

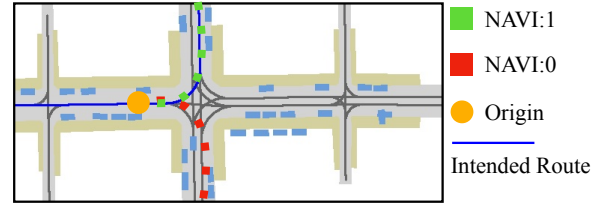


Fig. 2. Illustration of Navigation Compliance: the blue lines are the lane sets on route, two evaluated trajectories colored with red and green are depicted. The green path ends on route hence has the navigation compliance of 1, while the red path ends off route hence it has navigation compliance of 0.

input into the hydra scorer to predict the score for each metric. For each metric $m \in M$, we utilize a dedicated Multilayer Perceptron (MLP) to predict the scores $\{\hat{\mathbf{S}}_i^m\}_{i=1}^{N_t}$. Additionally, we predict the imitation score (im) $\{\hat{\mathbf{S}}_i^{im}\}_{i=1}^{N_t}$ similar to Hydra-MDP [1].

c) *Loss terms.*: The model is optimized using a weighted sum of loss terms, aligning the predictions of each sub-score and their ground-truth simulation scores as follows:

$$\mathcal{L} = \sum_{m \in M \cup \{im\}} \sum_{i=1}^{N_t} k_m \mathcal{L}_m(\hat{\mathbf{S}}_i^m, \mathbf{S}_i^m), \quad (4)$$

where k_m and \mathcal{L}_m are the weighting factor and loss function type for each sub-score m , N_t is the number of trajectory proposals, $\hat{\mathbf{S}}_i^m$ and \mathbf{S}_i^m are the prediction and simulation scores of sub-score m for i -th trajectory proposal. We apply a Binary Cross Entropy (BCE) Loss for binary sub-scores $M_{binary} = \{NC, DAC, TTC, C, NAVI\}$ and a Mean Squared Error (MSE) Loss for EP . To supervise the prediction of imitation score (im), we follow the approach outlined in Hydra-MDP [1], learning from the L2 distance between the expert trajectory and various trajectory proposals.

D. Inference

At inference time, we compose the output trajectory based on the predicted scores $\{\hat{\mathbf{S}}_i^m\}_{i=1}^{N_t}$. Since different scorers are trained using different loss functions, the distributions of the predicted scores vary. To align different sub-scores into a common distribution, we apply the following post-processing:

$$\mathcal{S}_i^m = \Phi(\hat{\mathbf{S}}_i^m), m \in M_{binary} \quad (5)$$

$$\mathcal{S}_i^m = \frac{\hat{\mathbf{S}}_i^m - \mu(\{\hat{\mathbf{S}}_i^m\}_{i=1}^{N_t})}{\sigma(\{\hat{\mathbf{S}}_i^m\}_{i=1}^{N_t})}, m \in M_{continuous} \quad (6)$$

where μ and σ represent the mean and standard deviation of input sub-scores. For binary sub-scores in $M_{binary} = \{NC, DAC, TTC, C, NAVI\}$, the sigmoid function Φ enhances their bimodal characteristics and preserves the original probabilistic interpretation of the scores. This normalization allows for a more straightforward comparison of scores when selecting the final trajectory. For continuous sub-scores in $M_{continuous} = \{EP, im\}$, we adjust the distribution to have a mean of 0 and a variance of 1, closing the gap with the range of the sigmoid function while preserving the original

distribution characteristics. Finally, we ensemble the different sub-scores using a weighting factor to form the final score for each trajectory proposal.

$$\mathcal{S}_i^{final} = \sum_{m \in M \cup \{im\}} w_m \mathcal{S}_i^m \quad (7)$$

We determine the optimal combination of weighting factors through a grid search, selecting the trajectory proposal with the highest final score as the model output.

IV. EXPERIMENTS

A. Datasets

a) *NAVSIM.*: We utilize NAVSIM [2] as our dataset for training and evaluation. The NAVSIM dataset is constructed based on the OpenScene [11] dataset, which is a redistribution of the nuPlan [8] dataset. In comparison to nuPlan, NAVSIM down-samples the sensor data to 2 Hz and includes only relevant annotations, such as 2D HD maps with semantic information and 3D bounding boxes for road participants. NAVSIM provides pre-selected training and testing splits, referred to **navtrain** and **navtest**, which contain 1,192 and 136 scenarios for training/validation and testing, respectively.

b) *Controllability evaluation.*: We select 121 scenarios with 1,884 samples from the **navtest** dataset to create the **navcontrol** split. This selection is strategically focused on scenarios that contain intersections, which is essential for assessing the controllability of the model, as it provides a context in which multiple navigation directions are possible. In contrast, we exclude scenes where only a single navigation direction is permitted, such as driving on a one-lane street where the only possible navigation command is to go straight. These scenarios do not adequately challenge the model's ability to interpret and respond to diverse navigation commands, thereby limiting the assessment of its controllability.

B. Metrics

a) *PDM score.*: The NAVSIM benchmark uses the PDM score to evaluate the closed-loop performance of the trajectory predictions, which is defined as:

$$PDM = NC \times DAC \times \frac{(5 \times TTC + 5 \times EP + 2 \times C)}{12}, \quad (8)$$

where NC, DAC, TTC, EP, C are the aforementioned closed-loop sub-scores. Additionally, we evaluate the model with NAVI metric to assess if the output trajectory follows the navigation route.

b) *Controllability measure.*: We propose a controllability measure (CM) to evaluate our method's ability to respond to different navigation command inputs. For each sample in **navcontrol**, we impose three different navigation commands as input. The output trajectory is evaluated using a kinetic-based function to determine if it aligns with the navigation command input, and the CM becomes:

$$CM = \sum_{d \in D} \sum_{c \in \{l, s, r\}} \kappa(T_c^d) * PDM(T_c^d), \quad (9)$$

where d represents a sample from the dataset D , $c \in \{Turn\ Left, Go\ Straight, Turn\ Right\}$ denotes a navigation command input, and T_c^d is the trajectory output for sample d with navigation command input c . The function κ is a simple kinetic-based binary classifier that validates whether the given trajectory matches its navigation command input. $PDM(T_c^d)$ denotes the PDM score of the trajectory T_c^d .

C. Baseline methods

PDM-closed [7] is a strong planner with privileged knowledge. We add UniAD [6], PARA-Drive [13] as they are well known end-to-end baselines. Hydra-MDP [1], [40] and Hydra-MDP++ [12]² both utilize hydra scorer to distill from the offline simulator. Transfuser [3] is a simple but effective transformer-based method. SSR [18] utilizes the SE-layer to fuse the navigation command into BEV feature, thus being a comparable baseline of our method. For Transfuser, we execute all benchmarks using the official checkpoint. For SSR, we retrain the model based on the official code using the **navtrain** dataset. We replace BEVFormer [16] with BEVFusion [14] as the BEV encoder for SSR to leverage additional LiDAR information for fair comparison.

D. Implementation details

The model is trained on the **navtrain** split using 8 V100 GPU with a batch size of 8 across 20 epochs. The initial learning rate is 1×10^{-5} and has an exponential weight decay to 1×10^{-6} in 20 epochs, and gradient clipping with 0.5 magnitude. We employ BEVFusion [14] as our perception backbone and adopt the same image resolution of 256×704 with 8 surrounding cameras provided in NAVSIM.

E. NAVSIM evaluation

a) *Quantitative comparison.*: Results can be found in Table I. Our method demonstrates SotA performance in terms of PDM score. Specifically, compared to Hydra-MDP++ \mathcal{V}_{8192} [12] and Hydra-MDP- \mathcal{V}_{16384} [40], we utilize 4096 trajectory proposals instead of 8192 or 16384, yet achieve a higher PDM score. Notably, we score marginally higher ego progress while maintaining competitiveness in other metrics, highlighting our model's exceptional safety and efficient driving behavior, profited from our novel trajectory decoder design.

b) *Qualitative comparison.*: We present a qualitative comparison of SSR [18], Transfuser [3], Hydra-MDP [40] and our method in Fig. 3. Our approach demonstrates superior performance in terms of both safety and navigation compliance indicated by the PDM score and NAVI score.

F. Controllability test

In this subsection, we showcase our model's controllability performance compared with SSR, Transfuser and Hydra-MDP, where SSR adopts a SE-layer to fuse the navigation command into the BEV feature. Transfuser and Hydra-MDP simply concatenate the navigation command as part of the ego status to the BEV feature and the trajectory feature.

²We report the result of Hydra-MDP++ from their paper since it is not open-sourced. We use the open-source Hydra-MDP- \mathcal{V}_{16384} for comparison.

TABLE I
QUANTITATIVE COMPARISON IN NAVTEST SPLIT OF NAVSIM BENCHMARK.

| Method | Inputs | NC↑ | DAC↑ | EP↑ | TTC↑ | C↑ | PDM Score↑ |
|---|----------------|-------------|-------------|-------------|-------------|------|-------------|
| PDM-Closed [7] | Perception GT | 94.6 | 99.8 | 89.9 | 86.9 | 99.9 | 89.1 |
| SSR† [18] | LiDAR & Camera | 90.7 | 83.8 | 66.8 | 82.3 | 100 | 69.1 |
| Transfuser* [3] | LiDAR & Camera | 97.8 | 92.1 | 78.6 | 92.8 | 100 | 83.4 |
| UniAD [6] | Camera | 97.8 | 91.9 | 78.8 | 92.9 | 100 | 83.4 |
| PARA-Drive [13] | Camera | 97.9 | 92.4 | 79.3 | 93.0 | 99.8 | 84.0 |
| Hydra-MDP- \mathcal{V}_{16384} * [40] | Camera | 98.5 | 98.8 | 85.4 | 94.9 | 100 | 90.8 |
| Hydra-MDP++ \mathcal{V}_{8192} [12] | Camera | <u>98.6</u> | <u>98.6</u> | <u>85.7</u> | <u>95.1</u> | 100 | <u>91.0</u> |
| Ours- \mathcal{V}_{4096} | LiDAR & Camera | 98.7 | <u>98.6</u> | 88.7 | 96.2 | 100 | 92.7 |

†We retrain the SSR model on **navtrain** split. * Evaluated using the official checkpoint.

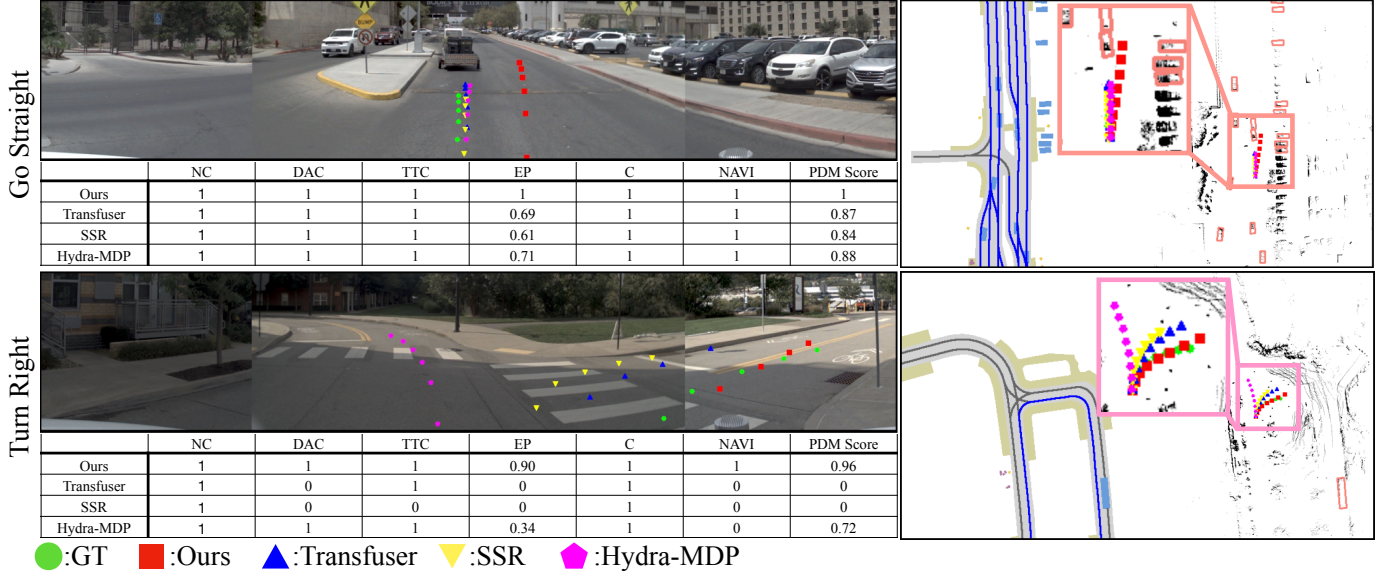


Fig. 3. Qualitative comparison of 2 selected scenes in **navtest** split. Input navigation commands are listed on the left. Routes are displayed as blue lines in the semantic map. Additionally, PDM scores along with other sub-scores for the evaluated trajectories are provided. Our trajectory achieves the highest PDM-score and demonstrates the best alignment with the navigation command.

TABLE II
CONTROLLABILITY EVALUATION IN NAVCONTROL SPLIT.

| Method | NC↑ | DAC↑ | EP↑ | TTC↑ | C↑ | PDM Score↑ | CM↑ |
|---------------------------------------|-------------|-------------|-------------|-------------|------------|-------------|-------------|
| SSR [18] | 74.1 | 46.2 | 29.2 | 62.7 | 100 | 32.7 | 22.6 |
| Transfuser [3] | 93.2 | 84.6 | 67.2 | <u>85.5</u> | 99.9 | 71.7 | 22.8 |
| Hydra-MDP- \mathcal{V}_{16384} [40] | 97.2 | 98.8 | 81.6 | 92.2 | 100 | 88.0 | 28.3 |
| Ours- \mathcal{V}_{4096} | 98.1 | 99.7 | 94.2 | 85.1 | 99.9 | 91.4 | 36.2 |

a) *Quantitative evaluation.*: The quantitative comparison of controllability is presented in Tab. II. Compared with other methods, our method achieves the highest CM score.

b) *Qualitative evaluation.*: Depicted in Fig. 4, we provide visualizations of 2 selected samples from **navcontrol**. Our method demonstrates high driving safety and controllability, benefiting from the design of navigation compliance. Hydra-MDP, without using navigation compliance as a supervision signal, fails to respond correctly towards the input navigation commands. Transfuser and SSR, while following the naviga-

tion commands, fall short of drivable area compliance.

c) *Corner cases.*: Furthermore, we analyze the corner cases to assess the model performance when the bad navigation command is imposed. Specifically, as shown in Fig. 5, going straight is not possible in that scenario. While SSR blindly following the navigation command, our method, disobeying the navigation command, chooses to turn left to avoid an erratic trajectory, displaying a safe behavior when facing a contradictory navigation command. For Transfuser and Hydra-MDP, despite turning left as well when imposed

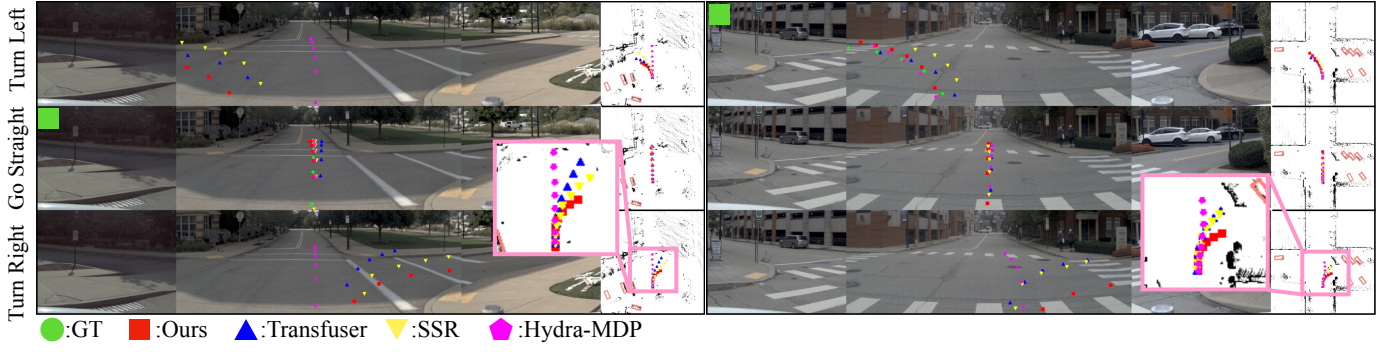


Fig. 4. Qualitative comparison of controllability test in **navcontrol** split. We present two scenarios, each of them is evaluated with 3 different navigation commands (Turn Left, Go Straight, Turn Right) as input. Only the scene corresponding to the original navigation command displays the ground truth trajectory, which is annotated with a green box.

TABLE III
ABLATION STUDIES OF VARIOUS MODEL COMPONENTS IN NAVTEST SPLIT.

| ID | Method | Modules | | | Metrics | | | | | | |
|----|---------------------------------------|--------------|--------------|----------------|---------------|----------------|---------------|----------------|--------------|-----------------|----------------------|
| | | Cmd | NAVI loss | Traj gathering | NC \uparrow | DAC \uparrow | EP \uparrow | TTC \uparrow | C \uparrow | NAVI \uparrow | PDM Score \uparrow |
| 1 | SSR [18] | - | - | - | 90.7 | 83.8 | 66.8 | 82.3 | 100 | 90.7 | 69.1 |
| 2 | Transfuser [3] | - | - | - | 97.8 | 92.1 | 78.6 | 92.8 | 100 | 96.9 | 83.4 |
| 3 | Hydra-MDP- \mathcal{V}_{16384} [40] | - | - | - | <u>98.5</u> | 98.8 | 85.4 | 94.9 | 100 | 97.7 | 90.8 |
| 4 | Ours- \mathcal{V}_{4096} | \times | \times | \checkmark | 98.0 | 98.1 | 88.1 | 95.0 | 100 | 89.6 | 91.6 |
| 5 | Ours- \mathcal{V}_{4096} | \checkmark | \times | \checkmark | 98.4 | 98.3 | 88.2 | <u>95.8</u> | 100 | 97.8 | <u>92.1</u> |
| 6 | Ours- \mathcal{V}_{4096} | \checkmark | \checkmark | \times | 98.4 | 98.2 | 83.9 | 95.5 | 100 | 98.9 | 89.5 |
| 7 | Ours- \mathcal{V}_{4096} | \checkmark | \checkmark | \checkmark | 98.7 | <u>98.6</u> | 88.8 | 96.2 | 100 | <u>98.0</u> | 92.7 |

going straight command, they do not react towards the turning right navigation command.

G. Ablation studies

We conduct several ablation studies in Tab. III using PDM-evaluation in **navtest** split and Tab. IV using controllability test in **navcontrol** split to validate the effectiveness of the following building blocks.

a) *Integrating navigation command.*: Depicted in Tab. III between ID 4 and 5, integrating the navigation command using a SE-layer in conjunction with the BEV feature is shown to have a positive effect, improving the PDM score by 0.5, NAVI by 8.2. For controllability test, the integration of navigation command is shown to significantly improve CM and PDM-Score as documented in Tab. IV between ID 1 and 2.

b) *Navigation compliance loss.*: Shown in Tab. III between ID 5 and 7, incorporating the NAVI loss introduced in Sec. III-C, increases the PDM score by 0.6, highlighting the effectiveness of utilizing navigation compliance loss. For controllability test, we evaluate the model performance w/o NAVI loss between ID 2 and 4 in Tab. IV. The CM and PDM-Score are overall improved after incorporating the NAVI loss, demonstrating the positive impact of this building block facing alternative navigation commands.

c) *Trajectory gathering.*: Illustrated by ID 6 and 7 in Tab. III and ID 3 and 4 in Tab. IV, we observe a significant improvement in both PDM-score and the controllability measure after incorporating the trajectory gathering method

TABLE IV
ABLATION STUDIES OF CONTROLLABILITY TEST IN NAVCONTROL SPLIT.

| ID | Modules | | | PDM Score \uparrow | CM \uparrow |
|----|--------------|--------------|----------------|----------------------|---------------|
| | Cmd | NAVI loss | Traj gathering | | |
| 1 | \times | \times | \checkmark | 87.8 | 22.5 |
| 2 | \checkmark | \times | \checkmark | 89.1 | 31.3 |
| 3 | \checkmark | \checkmark | \times | 87.6 | 29.9 |
| 4 | \checkmark | \checkmark | \checkmark | 91.4 | 36.2 |

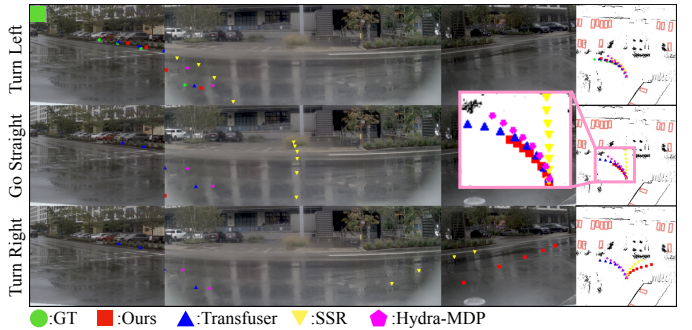


Fig. 5. Qualitative comparison when given a contradictory navigation command. We present a corner case in which going straight is not possible, while turning left or right are valid safe maneuvers. The original command is turning left.

introduced in Sec. III-B, showcasing that the gathering technique enhances the trajectory feature extraction, which leads

to performance improvement.

V. CONCLUSION AND FUTURE WORK

In this paper, we present NaviHydra, a novel end-to-end autonomous driving framework that effectively addresses the challenges of navigation controllability in E2EAD. By leveraging a BEV representation, our method enhances the model’s ability to process environmental information and provide context- and position-aware features. We introduced a robust trajectory gathering method that significantly improves trajectory feature extraction. The integration of high-level navigation commands as control signals allows for a stronger response to navigation inputs, closing the gap between the generalizability of end-to-end models and the controllability of rule-based planners. Additionally, our navigation compliance metric improves the alignment between generated trajectories and intended navigation commands, enhancing the planning performance of the system. The extensive experiments conducted on the NAVSIM dataset demonstrate that NaviHydra achieves SotA results, outperforming existing methods in both safety and controllability.

Future investigations include further improving the model’s adaptability to more fine-grind natural-language-based navigation commands and exploring the integration of VLMs to enhance decision-making capabilities under corner cases.

REFERENCES

- [1] Li, Z., Li, K., Wang, S., Lan, S., Yu, Z., Ji, Y., Li, Z., Zhu, Z., Kautz, J., Wu, Z. & Others Hydra-MDP: End-to-end Multimodal Planning with Multi-target Hydra-Distillation. *ArXiv Preprint ArXiv:2406.06978*. (2024)
- [2] Dauner, D., Hallgarten, M., Li, T., Weng, X., Huang, Z., Yang, Z., Li, H., Gilitschenski, I., Ivanovic, B., Pavone, M., Geiger, A. & Chitta, K. NAVSIM: Data-Driven Non-Reactive Autonomous Vehicle Simulation and Benchmarking. *NeurIPS*. (2024)
- [3] Chitta, K., Prakash, A., Jaeger, B., Yu, Z., Renz, K. & Geiger, A. Transfuser: Imitation with transformer-based sensor fusion for autonomous driving. *TPAMI*. (2022)
- [4] Jiang, B., Chen, S., Xu, Q., Liao, B., Chen, J., Zhou, H., Zhang, Q., Liu, W., Huang, C. & Wang, X. Vad: Vectorized scene representation for efficient autonomous driving. *ICCV*. (2023)
- [5] Chen, S., Jiang, B., Gao, H., Liao, B., Xu, Q., Zhang, Q., Huang, C., Liu, W. & Wang, X. VADv2: End-to-End Vectorized Autonomous Driving via Probabilistic Planning. *ArXiv Preprint ArXiv:2402.13243*. (2024)
- [6] Hu, Y., Yang, J., Chen, L., Li, K., Sima, C., Zhu, X., Chai, S., Du, S., Lin, T., Wang, W. & Others Planning-oriented autonomous driving. *CVPR*. (2023)
- [7] Dauner, D., Hallgarten, M., Geiger, A. & Chitta, K. Parting with misconceptions about learning-based vehicle motion planning. *CoRL*. (2023)
- [8] H. Caesar, K. NuPlan: A closed-loop ML-based planning benchmark for autonomous vehicles. *CVPR ADP3 Workshop*. (2021)
- [9] Yang, L., Kang, B., Huang, Z., Xu, X., Feng, J. & Zhao, H. Depth anything: Unleashing the power of large-scale unlabeled data. *ArXiv Preprint ArXiv:2401.10891*. (2024)
- [10] Li, Z., Yu, Z., Lan, S., Li, J., Kautz, J., Lu, T. & Alvarez, J. Is Ego Status All You Need for Open-Loop End-to-End Autonomous Driving?. *ArXiv Preprint ArXiv:2312.03031*. (2023)
- [11] Contributors, O. OpenScene: The Largest Up-to-Date 3D Occupancy Prediction Benchmark in Autonomous Driving. (<https://github.com/OpenDriveLab/OpenScene>, 2023)
- [12] Li, K., Li, Z., Lan, S., Xie, Y., Zhang, Z., Liu, J., Wu, Z., Yu, Z. & Alvarez, J. Hydra-MDP++: Advancing End-to-End Driving via Expert-Guided Hydra-Distillation. (2025), <https://arxiv.org/abs/2503.12820>
- [13] Weng, X., Ivanovic, B., Wang, Y., Wang, Y. & Pavone, M. Parade: Parallelized architecture for real-time autonomous driving. *CVPR*. (2024)
- [14] Liu, Z., Tang, H., Amini, A., Yang, X., Mao, H., Rus, D. & Han, S. BEVFusion: Multi-Task Multi-Sensor Fusion with Unified Bird’s-Eye View Representation. *ICRA*. (2023)
- [15] Hu, J., Shen, L. & Sun, G. Squeeze-and-Excitation Networks. *CoRR*. **abs/1709.01507** (2017), <http://arxiv.org/abs/1709.01507>
- [16] Li, Z., Wang, W., Li, H., Xie, E., Sima, C., Lu, T., Yu, Q. & Dai, J. Bevformer: learning bird’s-eye-view representation from lidar-camera via spatiotemporal transformers. *TPAMI*. (2024)
- [17] Winter, K., Azer, M. & Flohr, F. BEVDriver: Leveraging BEV Maps in LLMs for Robust Closed-Loop Driving. *ArXiv Preprint ArXiv:2503.03074*. (2025)
- [18] Li, P. & Cui, D. Navigation-Guided Sparse Scene Representation for End-to-End Autonomous Driving. *ICLR*. (2025)
- [19] Pan, B., Sun, J., Leung, H., Andonian, A. & Zhou, B. Cross-view semantic segmentation for sensing surroundings. *IEEE Robotics And Automation Letters*. (2020)
- [20] Philion, J. & Fidler, S. Lift, splat, shoot: Encoding images from arbitrary camera rigs by implicitly unprojecting to 3d. *ECCV*. (2020)
- [21] Ma, W., Jiang, J., Yang, Y., Chen, Z. & Chen, H. LSSInst: Improving Geometric Modeling in LSS-Based BEV Perception with Instance Representation. *3DV*. (2025)
- [22] Liu, Y., Wang, T., Zhang, X. & Sun, J. Petr: Position embedding transformation for multi-view 3d object detection. *ECCV*. (2022)
- [23] Zhou, B. & Krähenbühl, P. Cross-view transformers for real-time map-view semantic segmentation. *CVPR*. (2022)
- [24] Yang, C., Chen, Y., Tian, H., Tao, C., Zhu, X., Zhang, Z., Huang, G., Li, H., Qiao, Y., Lu, L. & Others Bevformer v2: Adapting modern image backbones to bird’s-eye-view recognition via perspective supervision. *CVPR*. (2023)
- [25] Qin, Z., Chen, J., Chen, C., Chen, X. & Li, X. Unifusion: Unified multi-view fusion transformer for spatial-temporal representation in bird’s-eye-view. *ICCV*. (2023)
- [26] Gu, S., Yin, W., Jin, B., Guo, X., Wang, J., Li, H., Zhang, Q. & Long, X. Dome: Taming diffusion model into high-fidelity controllable occupancy world model. *ArXiv Preprint ArXiv:2410.10429*. (2024)
- [27] Wang, P., Zhu, M., Zheng, X., Lu, H., Zhong, H., Chen, X., Shen, S., Wang, X., Wang, Y. & Wang, F. Bevgpt: Generative pre-trained foundation model for autonomous driving prediction, decision-making, and planning. *IEEE Transactions On Intelligent Vehicles*. (2024)
- [28] Wei, J., Yuan, S., Li, P., Hu, Q., Gan, Z. & Ding, W. Occllama: An occupancy-language-action generative world model for autonomous driving. *ArXiv Preprint ArXiv:2409.03272*. (2024)
- [29] Treiber, M., Hennecke, A. & Helbing, D. Congested traffic states in empirical observations and microscopic simulations. *Phys. Rev. E*. **62**, 1805-1824 (2000,8), <https://link.aps.org/doi/10.1103/PhysRevE.62.1805>
- [30] Li, Y., Fan, L., He, J., Wang, Y., Chen, Y., Zhang, Z. & Tan, T. Enhancing End-to-End Autonomous Driving with Latent World Model. *ICLR*. (2025)
- [31] Hamdan, S. & Güney, F. Carformer: Self-driving with learned object-centric representations. *ECCV*. (2024)
- [32] Gao, H., Chen, S., Jiang, B., Liao, B., Shi, Y., Guo, X., Pu, Y., Yin, H., Li, X., Zhang, X., Zhang, Y., Liu, W., Zhang, Q. & Wang, X. RAD: Training an End-to-End Driving Policy via Large-Scale 3DGS-based Reinforcement Learning. *ArXiv Preprint ArXiv:2502.13144*. (2025)
- [33] Xing, Z., Zhang, X., Hu, Y., Jiang, B., He, T., Zhang, Q., Long, X. & Yin, W. GoalFlow: Goal-Driven Flow Matching for Multimodal Trajectories Generation in End-to-End Autonomous Driving. *CVPR*. (2025)
- [34] Li, Z., Wang, S., Lan, S., Yu, Z., Wu, Z. & Alvarez, J. Hydra-next: Robust closed-loop driving with open-loop training. *ArXiv Preprint ArXiv:2503.12030*. (2025)
- [35] Harley, A., Fang, Z., Li, J., Ambrus, R. & Fragkiadaki, K. Simple-BEV: What Really Matters for Multi-Sensor BEV Perception?. *ICRA*. (2023)
- [36] Zhang, Y., Zhu, Z., Zheng, W., Huang, J., Huang, G., Zhou, J. & Lu, J. BEVerse: Unified Perception and Prediction in Birds-Eye-View for Vision-Centric Autonomous Driving. *ArXiv Preprint ArXiv:2205.09743*. (2022)
- [37] Huang, J., Huang, G., Zhu, Z., Yun, Y. & Du, D. BEVDet: High-performance Multi-camera 3D Object Detection in Bird-Eye-View. *ArXiv Preprint ArXiv:2112.11790*. (2021)

- [38] Liang, T., Xie, H., Yu, K., Xia, Z., Lin, Z., Wang, Y., Tang, T., Wang, B. & Tang, Z. Bevfusion: A simple and robust lidar-camera fusion framework. *NeurIPS*. (2022)
- [39] Wang, H., Tang, H., Shi, S., Li, A., Li, Z., Schiele, B. & Wang, L. Unitr: A unified and efficient multi-modal transformer for bird's-eye-view representation. *ICCV*. (2023)
- [40] Li, Z., Yao, W., Wang, Z., Sun, X., Chen, J., Chang, N., Shen, M., Wu, Z., Lan, S. & Alvarez, J. Generalized Trajectory Scoring for End-to-end Multimodal Planning. *ArXiv Preprint ArXiv:2506.06664*. (2025)